JOURNAL OF OPTOELECTRONICS AND ADVANCED MATERIALS Vol. 10, No. 2, February 2008, p. 400 - 404

Optical and magnetic properties of $Zn_{1-x}Co_xO$ nanorod arrays fabricated by hydrothermal method

YALU ZUO, SHIHUI GE*, LI ZHANG, XUEYUN ZHOU, SHIMING YAN, YUHUA XIAO
Key Laboratory for Magnetism and Magnetic Materials of Ministry of Education, Lanzhou University, Lanzhou 730000, P.R. China

$Zn_{1-x}Co_xO$ (x = 0.1, 0.2) nanorods were prepared by hydrothermal method. The morphology of the nanorods was studied by field emission scanning electron microscopy. The results from x-ray diffraction and transmission microscopy indicate that the as-prepared nanorods have single-crystalline wurtzite structure, and no metallic Co or other secondary phases were found. The vibrating sample magnetometer measurement showed that $Zn_{0.8}Co_{0.2}O$ nanorods possess room temperature ferromagnetism (RTFM). The nanorods exhibit strong red emission as evidence by the photoluminescence spectra.

(Received December 17, 2007; accepted February 7, 2008)

Keywords: $Zn_{1-x}Co_xO$ nanorods, Room temperature ferromagnetism, Photoluminescence

1. Introduction

ZnO nanomaterials have been extensively investigated for applications in luminescence, photocatalysts, gas sensors, solar cells and so on due to their specific electrical and optoelectronic properties [1, 2]. The properties of ZnO nanomaterials strongly depend on their dimensions and morphologies. Therefore, an investigation of ZnO nanostructures in highly aligned and ordered arrays is of critical importance for the development of novel devices [3, 4].

For the growth of highly aligned ZnO nanostructures, gas-phase deposition is one of the principal technologies. Although this approach can produce high-quality aligned ZnO nanostructures, it needs high temperature and metal catalyst particles to direct the aligned growth. Moreover, these techniques consume a large amount of energy and require equipment with rigorous experimental conditions. Therefore, such limitations inspired the research on solution-phase synthesis, which offers a great potential for a low-cost and large-scale fabrication [5-8]. The low-temperature solution methods (<110◦C) are particularly attractive because of their low energy requirements, safe and environmentally benign synthetic conditions. Recently, Greene *et al* reported a two-step method for the growth of vertically aligned ZnO nanowires using a textured ZnO seed at 90◦C [9].

ZnO is a wide band gap semiconductor (3.37eV) which has a large exciton binding energy (60meV). Therefore, it is of great interest for practical applications in short wavelength photonic devices. In the photoluminescence (PL) spectra of ZnO, typically UV band-edge emission and one or more broad emission peaks in the visible range are observed. Among different visible emission peaks associated with defects, the green emission is the most common one [10]. However, ZnO nanostructures prepared by chemical methods typically exhibit yellow defect emission (centered at 580 nm) [11, 12].

Diluted magnetic semiconductors (DMSs) have attracted considerable research interest in recent years due to their great potential applications in spintronic devices [13-19]. Some results have been achieved concerning the room-temperature ferromagnetism in Co-doped ZnO films and aggregated nanocrystals [20, 21]. However, the synthesis and magnetic study of one dimensional Co-doped ZnO nanomaterials are still in a nascent stage [22, 23]. So, studies on fabrication in optical and magnetic properties of one dimensional Co-doped ZnO are interesting.

It is well known that the morphology of ZnO nanorods fabricated by hydrothermal methods is strongly dependent on the experimental conditions, such as solution concentration, growth temperature, and the substrate condition. However, the effects of the dopant ions during hydrothermal growth have not been studied in detail. In this work, we studied the influence of the solution concentration and Co doping on the morphology of fabricated ZnO nanorods. Furthermore, we investigated the the effect of dopant and annealing in forming gas (argon and hydrogen) on the optical properties of the nanorods.

2. Experimentals

High quality Co doped ZnO nanorods were synthesized by a simple hydrothermal route at low temperature (90°C). The ZnO nanorods were grown by

two steps. We first deposited ZnO seed layer on Si (100) substrates by the sol-gel method. Aqueous solutions of zinc acetate (0.5 M) and methenamine (0.5 M) were dripped on Si (100) substrates. After subsequent spin coating, the substrates were annealed at 400 °C for one hour. At least two cycles were needed for the dense and uniform dispersion of ZnO nanoparticles on Si (100) substrates. Then the films were put into a 50 ml Tefloni container with equimolar aqueous solution of zinc nitrate hexahydrate ($Zn(NO_3)_2{\cdot}6H_2O$) and having inside hexamethylenetetramine ($C_6H_{12}N_4$). The container was sealed with a cap and placed in an oven to carry out the hydrothermal growth at 90°C for 4 hours. Finally, the nanorod films were thoroughly washed with distilled water to eliminate residual salts, and dried in air at 60°C. By this way, a series of ZnO nanorod samples were prepared with different solution concentrations of 0.02M, 0.05M and 0.1M. In addition, we also fabricated $Zn_{1-x}Co_xO$ (x = 0.1, 0.2) nanorods by adding $Co(NO_3)_2{\cdot}6H_2O$ into aqueous solution.

X-ray diffraction (XRD), field emission scanning electron microscopy (FESEM) and transmission electron microscopy (TEM) were used to characterize the structures and morphology of the nanorod films. Raman spectroscopy was also conducted as a supplementary tool to identify structural information. The optical and magnetic properties of the Co-doped ZnO nanorods were investigated by Photoluminescence (PL) spectrometry and vibrating sample magnetometer (VSM), respectively.

3. Results and discussion

Fig1.a-c show the images of the undoped ZnO nanorods prepared with different solution concentration of 0.02M, 0.05M and 0.1M of $Zn(NO_3)_2{\cdot}6H_2O$ and $C_6H_{12}N_4$, respectively. It can be observed that the ZnO nanorods were grown successfully on substrates for different solution concentration. The cross-section image of as-prepared nanorods with solution concentration of 0.05M is shown in the inset of Fig.1b from which we note that all the nanorods grow vertically from the substrate and have a length of several hundred nanometers (about 500nm). Obviously, the solution concentration affects the nanorods morphology. The nanorods are grown perpendicularly over the whole substrate surface in Fig.1b (0.05M) and Fig. 1c (0.1M) while the nanorods are somewhat disordered in Fig.1a (0.02M). Otherwise, the diameter (about 50-80nm) of rods with 0.05M is samller and more uniform than that (80-200nm) with 0.1M. The small diameter and relatively large length result in a high aspect ratio which is favor of applications.

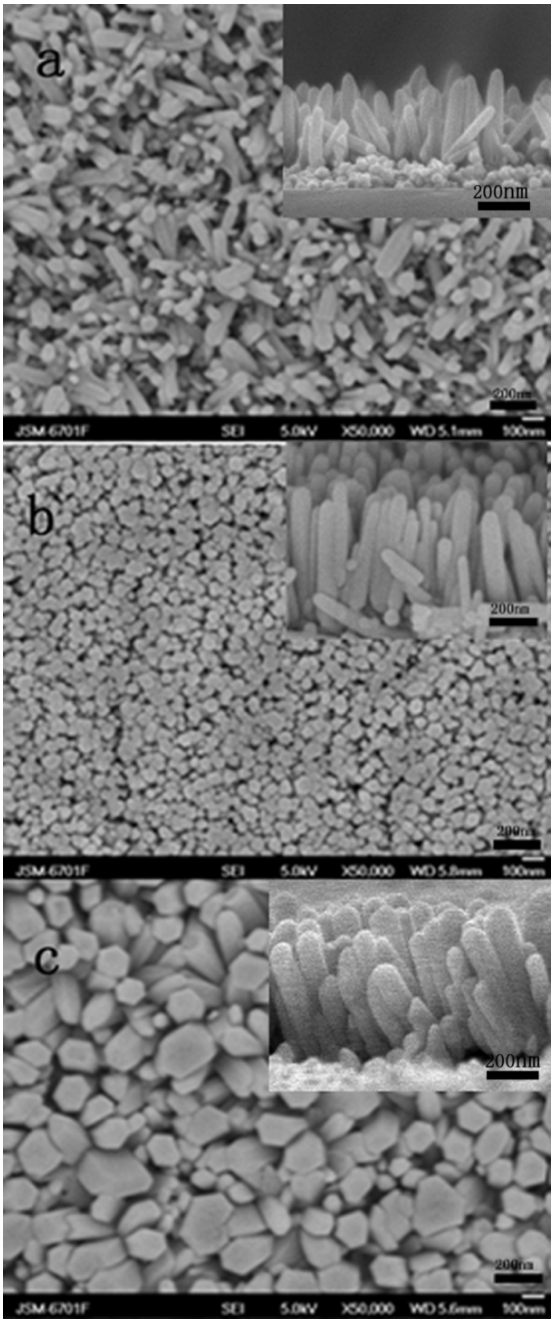

Fig. 1. FESEM images of the ZnO nanorod films grown on Si (100) substrates with different solution concentration.

From above results, the uniform and well-orient ZnO nanorod arrays can be prepared with 0.05M solution concentration. In the following we prepared $Zn_{1-x}Co_xO$ nanorods with this solution concentration. The FESEM images of the $Zn_{1-x}Co_xO$ nanorods prepared with nominal cobalt doping concentrations of 10% and 20% are shown in Fig.2a and Fig.2b. It can be seen that with cobalt doping, the nanorods are still uniform, well-orient and vertical to the substrate plane.

The XRD patterns show that all nanorod arrays have the wurtzite strucure of ZnO (hexagonal). Fig.3 shows the XRD patterns of pure ZnO and $Zn_{0.8}Co_{0.2}O$ nanorod arrays. All the diffraction peaks can be indexed to a ZnO wurtzite structure. Furthermore, no other impurity phase was found in XRD pattern of $Zn_{0.8}Co_{0.2}O$ nanorods, indicating that Co ions successfully occupy the lattice sites. The strong relative intensity of the (002) peak reveals a texture effect of the arrays consistent with *c*-axis oriented nanorods [24].

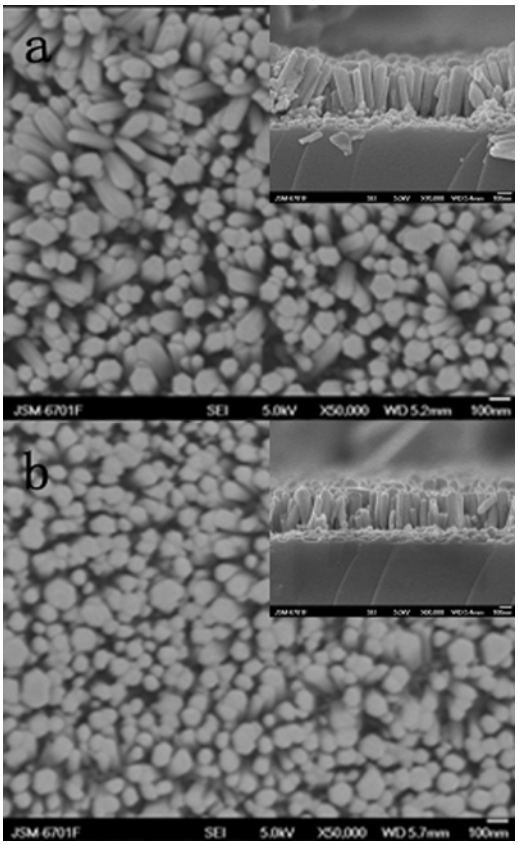

Fig. 2. FESEM images of the $Zn_{1-x}Co_xO$ nanorods with nominal Co concentration of x = 0.1 and x = 0.2.

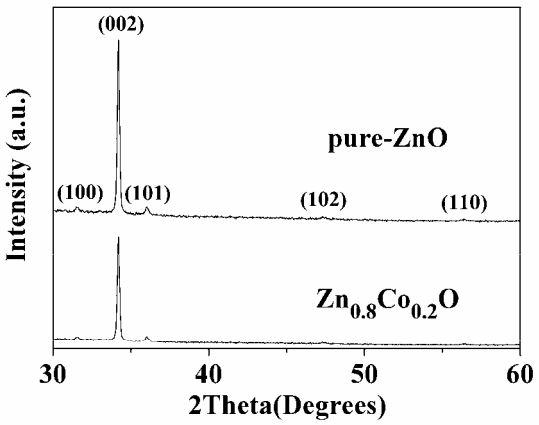

Fig. 3. XRD pattern of pure ZnO and $Zn_{0.8}Co_{0.2}O$ nanorod arrays.

The detailed structural characterization of the as-grown ZnO nanorod arrays was done by transmission electron microscopy (TEM). Fig.4 is a typical TEM image of one single $Zn_{0.8}Co_{0.2}O$ nanorod, its diameter is about 90 nm and length up to about 500nm. It is obvious that the nanorod has a clean and smooth surface, and its bottom is a ZnO seed layer prepared in the first step of sample preparation. The corresponding selected area electron diffraction (SAED) pattern (inset of Fig.4) can be indexed to the [001] axis diffraction pattern of wurtzite structured ZnO [25], which is consistent with XRD results. And no diffraction spots and rings denoting Co clusters or Co oxide phases were found.

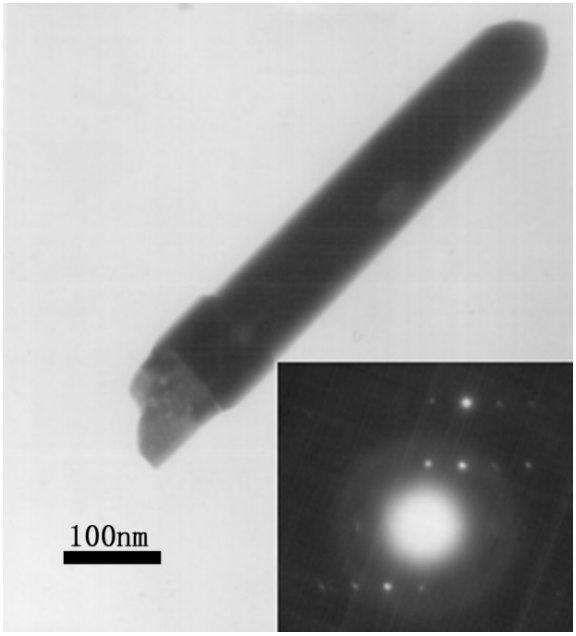

Fig. 4. Typical TEM image of one single $Zn_{0.8}Co_{0.2}O$ nanorod, inset is the corresponding SAED pattern.

Raman spectroscopy was conducted for ZnO nanorods to obtain the additional information for the film structure. Fig.5 shows the micro-Raman spectra of both pure ZnO and $Zn_{0.8}Co_{0.2}O$ nanorods at the range of 300–700 cm^{-1}. The E_2 (high) is known to be the band characteristic of the wurtzite phase [26]. The position of the E_2 (high) mode of the ZnO is observed at 439 cm^{-1} for pure ZnO and $Zn_{0.8}Co_{0.2}O$ nanorods. It can be seen obviously that the peak at 439 cm^{-1} lowers by doping cobalt into ZnO owing to the worse crystal structure. It can be considered as an evidence that Co dopant inhibits the growth of ZnO nanorods. Two more peaks located at 575 and 389 cm^{-1} are identified as the A_1 (LO) and A_1 (TO) phonon mode respectively. The A_1 mode is associated with the defects. The peak located at 525 cm^{-1} is come from Si (100) substrate. The 332 cm^{-1} mode is attributed to the second order Raman process [27].

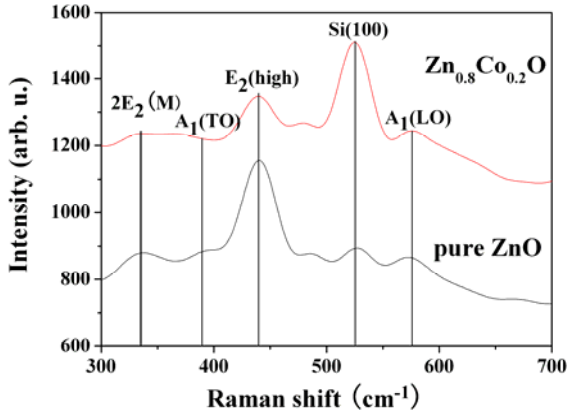

Fig. 5. Raman spectra of pure ZnO and $Zn_{0.8}Co_{0.2}O$ nanorods.

Fig. 6 presents the M-H curve of the $Zn_{0.8}Co_{0.2}O$ nanorods measured at 300K. The paramagnetic contribution has been subtracted and only the ferromagnetic property is shown. The M-H curve exhibits a hysteresis loops with a coercivity of 100 Oe and a saturation magnetization of 0.003emu/g. As to the origin of ferromagnetic behavior observed in Co doped ZnO nanorods, there are a few of controversial explanations, one of which is the formation of some nanoscale Co-related secondary phase, such as metallic Co precipitation and Co oxides. First, the origin from Co oxides can be easily ruled out, since bulk CoO and Co_3O_4 is antiferromagnetism with Neel temperature of 293K and 33K respectively. Secondly, the existence of metallic Co is also a unlike source of this ferromagnetism because the synthesis of Co-doped ZnO nanorods is performed in water as well as OH- environment which can prevent the formation of metallic Co nanoclusters to some extent. In addition, XRD and TEM results clearly show no metallic Co clusters and Co oxides in the nanorods. Thus ferromagnetism in the Co doped ZnO nanorods could be considered as a result of the exchange interaction between free delocalized carriers (holes or electrons from the valence band) and the localized *d* spins on the Co ions.

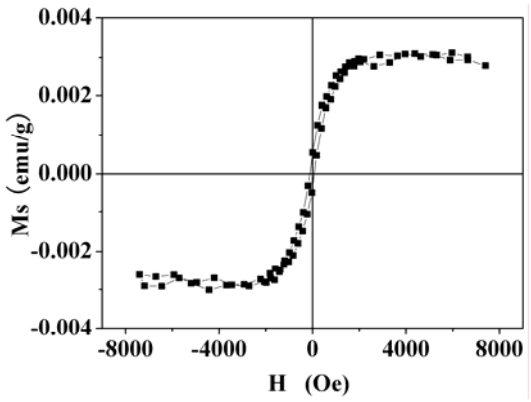

Fig. 6. Room temperature hysteresis loop of $Zn_{0.8}Co_{0.2}O$ nanorods.

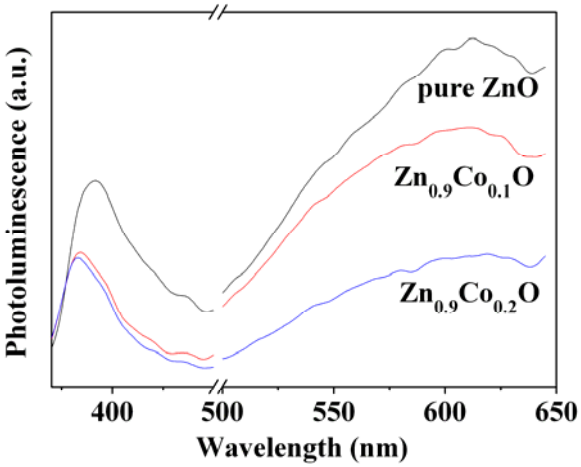

Fig. 7. PL spectra for pure ZnO, $Zn_{0.9}Co_{0.1}O$ and $Zn_{0.8}Co_{0.2}O$ nanorods taken at room temperature (λ_{ex} =325 nm).

Fig. 7 presents the room temperature photoluminescence spectra (λex =325nm) for pure ZnO, $ZnO_{0.9}Co_{0.1}O$ and $ZnO_{0.8}Co_{0.2}O$ nanorods. The figure exhibits strong near band edge UV emission peaks centered at 391 nm, and noticeably, broad strong red emissions centered at about 613 nm.

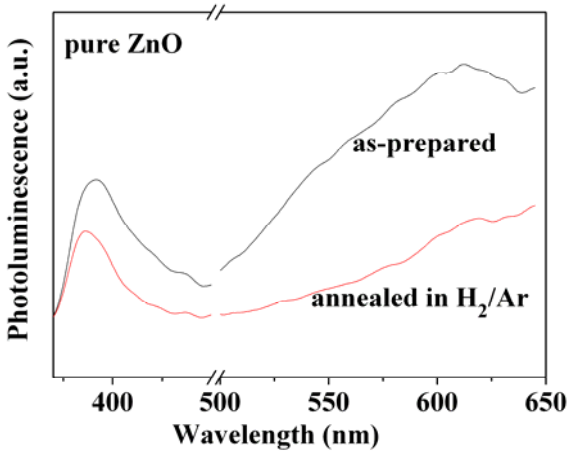

Fig. 8. PL spectra for as-prepared and annealed samples in forming gas of pure ZnO nanorods taken at room temperature (λ_{ex} = 325nm).

It is known that the green emission results from the recombination of electrons with holes trapped in singly ionized oxygen vacancies and is commonly seen in ZnO materials synthesized under oxygen-deficient conditions [28]. The red emission is less commonly reported, and its origin, although not fully understood, seems to involve the presence of interstitial oxygen defects. Compared with the spectrum of pure ZnO, the red emission peak intensities decrease in $ZnO_{0.9}Co_{0.1}O$ and $ZnO_{0.8}Co_{0.2}O$ nanorods, a possibility for this behavior is that the dopants reduce the

quantity of interstitial oxygen defects.

In order to verify whether the red emission indeed originates from the interstitial oxygen defects, we performed an investigation on the annealing effect. The samples were annealed in forming gas of argon (90%) and hydrogen (10%) at 400°C for 10 minutes, and then the red spectra were taken at RT. The result for pure ZnO nanorods is shown in Fig.8. It can be seen that the annealing in forming gas results in reduction of red emission. The annealing for $ZnO_{0.9}Co_{0.1}O$ and $ZnO_{0.8}Co_{0.2}O$ nanorods obtained the same results. This behavior could be understood as following: the hydrogen can assist the removal of excess oxygen, which would result in reduced defect emission.

4. Conclusions

$Zn_{1-x}Co_xO$ nanorods were fabricated by a hydrothermal method from aqueous solutions of zinc nitrate hydrate, Cobalt nitrate hydrate and hexamethylenetetramine. All of the as-prepared samples were single-crystalline wurtzite structure, and no metallic Co or other secondary phases were found. $Zn_{1-x}Co_xO$ nanorods exhibit room temperature ferromagnetism (RTFM). The PL spectra of pure ZnO and the $Zn_{1-x}Co_xO$ nanorods exhibit typical UV emission and red emission. Moreover, it is observed that annealing in forming gas results in reduction of red emission.

Acknowledgment

This work is supported by National Natural Science Foundation of China (NO.50371034).

References

[1] D. C. Look, Mater. Sci. Eng.B-Solid-State Mater. Adv. Technol. **80**, 383 (2001).
[2] Z. R. Tian, J. A. Voigt, J. Liu, B. Mckenzie, M. J. Mcdermott, M. A. Rodriguez, H. Konishi, H. Xu, Nat. Mater. **2**, 821 (2003).
[3] M. H. Huang, S. Mao, H. Feick, H. Yan, Y. Wu, H. Kind, E. Weber, R. Russo, P. Yang, Science. **292**, 1897 (2001).
[4] N. Beermann, L. Vayssieres, S.E. Lindquist, A.J. Hagfeldt, Electrochem. Soc. **147**, 2456 (2000).
[5] L.E. Greene, M. Law, J. Goldberger, F. Kim, J.C. Johnson, Y. Zhang, R.J. Saykally, P. Yang, Angew. Chem. Int. Ed. **42**, 3031 (2003).
[6] D. Li, Y.H. Leung, A.B. Djurisˇ icʹ, Z.T. Liu, M.H. Xie, S.L. Shi, S.J. Xu, W.K. Chan, Appl. Phys. Lett. **85**, 1601 (2004).
[7] L. Vayssieres, Int. J. Mater. Product Technol. **18**, 330 (2003).
[8] M. Law, L.E. Greene, J.C. Johnson, R. Saykally, P. Yang, Nat. Mater. **4**, 455 (2005).
[9] L E. Greene, M. Law, D. H. Tan, M. Montano, J. Goldberger, G. Somorjai, P. Yang, Nano. lett. **5**, 1231 (2005).
[10] A.B. Djurisˇ icʹ , W.C.H. Choy, V.A.L. Roy, Y.H. Leung, C.Y. Kwong, K.W. Cheah, T.K. Gundu Rao, W.K. Chan, H.F. Lui, C. Surya, Adv. Funct. Mater. **14**, 856 (2004).
[11] L.E. Greene, M. Law, J. Goldberger, F. Kim, J.C. Johnson, Y. Zhang, R.J. Saykally, P. Yang, Angew. Chem. Int. Ed. **42**, 3031 (2003).
[12] D. Li, Y.H. Leung, A. B. Djurisˇ icʹ , Z.T. Liu, M.H. Xie, S.L. Shi, S.J. Xu, W.K. Chan, Appl. Phys. Lett. **85**, 1601 (2004).
[13] S. D. Sarma, Nat. Mater. **2**, 292 (2003).
[14] S. J. Pearton, C. R. Abernathy, M. E. Overberg, G. T. Thaler, A. F. Hebard, Y. D. Park, F. Ren, J. Kim, L. A. Boatner, J. Appl. Phys. **1**, 93 (2003).
[15] H. Akinaga, H. Ohno, IEEE Trans Nanotechnol. **1**, 19 (2002).
[16] T. Dietl, Semicond. Sci. Technol. **17**, 377 (2002).
[17] I. Malajovich, J. J. Berry, N. Samarth, D. D. Awshalom, Nature. **411**, 770 (2001).
[18] H. Ohno, Science. **281**, 951 (1998).
[19] S. A. Wolf,D. D. Awschalom,R. A. Buhrman, J. M. Daughton,S.Von Molnar, M. L. Roukes, A.Y. Chtehelkanova, D. M. Treger, Science. **294**, 1488 (2001).
[20] Jae. Hyun. Kim, Hyojin. Kim, Dojin. Kim, Soon. Gil. Yoon and Woong. Kil. Choo, Solid State Communications. **131**, 677 (2004).
[21] Dana A. Schwartz, Nick S. Norberg, Quyen P. Nguyen, Jason M. Parker, and Daniel R. Gamelin, J. Am. Chem. Soc. **125**, 13205 (2003).
[22] J. B. Cui, Q. Zeng, U. J. Gibson, J. Appl. Phys. **99**, 08M113 (2006).
[23] J. B. Cui, U. J. Gibson. Appl. Phys. Lett. **87**, 133108 (2005).
[24] Q Ahsanulhaq, A Umar, Y B Hahn, Nanotechnology. **18**, 115603 (2007)
[25] Min Guo, Peng Diaoc, Shengmin Cai, Applied Surface Science. **249**, 71 (2005).
[26] Sang-Hun Jeong, Jae-keun Kim and Byung-Teak Lee, J. Phys. D: Appl. Phys. **36**, 2017 (2003).
[27] Z. Q. Chen, A. Kawasuso, Y. Xu, H. Naramoto, X. L. Yuan, T. Sekiguchi, R. Suzuki, T. Ohdaira, J. Appl. Phys. **97**, 013528 (2005).
[28] J. C. Johnson, H. Yan, P. Yang, R. J. Saykally, J. Phys. Chem. B **107**, 8816 (2003).

*Corresponding author: gesh@ lzu.edu.cn; zuoyl04@yahoo.cn